GLM-Regularized Low-Rank Factorization For Extracting Functional Response From Swept-3D Functional Ultrasound

Erol, Aybuke; Generowicz, Bastian; Kruizinga, Pieter; Hunyadi, Borbala

DOI
10.1109/ICASSPW59220.2023.10193574

Publication date
2023

Document Version
Final published version

Published in
ICASSPW 2023 - 2023 IEEE International Conference on Acoustics, Speech and Signal Processing Workshops, Proceedings

2023 IEEE International Conference on Acoustics, Speech, and Signal Processing Workshops (ICASSPW) | 979-8-3503-0261-5/23/$31.00 ©2023 IEEE | DOI: 10.1109/ICASSPW59220.2023.10193574

GLM-REGULARIZED LOW-RANK FACTORIZATION FOR EXTRACTING FUNCTIONAL RESPONSE FROM SWEPT-3D FUNCTIONAL ULTRASOUND

Aybüke Erol[1], *Bastian Generowicz*[2], *Pieter Kruizinga*[2], *Borbála Hunyadi*[1]

[1]Signal Processing Systems (SPS), Delft University of Technology, Delft, The Netherlands
[2]Department of Neuroscience, Erasmus Medical Center, Rotterdam, The Netherlands

ABSTRACT

Functional ultrasound (fUS) is an emerging neuroimaging modality that indirectly measures neural activity by detecting fluctuations in local blood dynamics. fUS acquisitions typically rely on the use of a 1D array transducer, which records hemodynamic activity in a single plane. A new technique named swept-3D fUS imaging obtains a full 3D volume of the brain by continuously moving a 1D array back-and-forth over the volume of interest. The standard procedure in fUS imaging involves filtering and averaging a number of ultrasound frames obtained at a single location to compute power-Doppler images, yet, in case of swept-3D fUS, the location of the recorded slice shifts at each time instant due to probe motion. In this work, we aim at discovering task-relevant components from 3D fUS data while taking into account the spatiotemporal differences in adjacent slices. We propose an alternating optimization scheme with general liner model-based regularization, and validate our method on swept-3D fUS data by identifying active regions and time traces within the mouse brain during a visual experiment.

***Index Terms*—** 3D functional ultrasound, regularized factorization, mouse, brain

1. INTRODUCTION

Functional ultrasound (fUS), similar to functional magnetic resonance imaging (fMRI), is a hemodynamics-based neuroimaging technique. fUS can detect subtle variations in blood volume, which, through neurovascular coupling, constitutes an indirect measure for neural activity [1]. More precisely, local changes in neural activity induce a delayed response in blood flow and volume, which can be modelled by the impulse response of the underlying neurovascular system, named as the hemodynamic response function (HRF) [2]. The HRF exerts a low-pass filtering effect on the neural activity, and as such, mostly the low-frequency content of the fUS signal is known to be correlated with neural activity [3].

Traditionally, fUS makes use of tilted plane waves transmitted through the brain via a linear array transducer. After beamforming of the backscattered echoes and angular-compounding, a 2D compound image is acquired for a brain slice at approximately every 1 ms. Next, batches of (typically around 200) compound images are grouped, and the Doppler power-per-voxel is computed within each batch by separating the blood signal from tissue components using singular value decomposition (SVD)-filtering [4], giving rise to Power-Doppler Images (PDIs) [5].

When imaging the full 3D brain with fUS, one way is to concatenate 2D fUS images of different slices by repeating the same experiment at each slice [6], which notably prolongs the recording time. Alternatively, a 2D matrix array can be used for ultrasound transmission [7], which demands more expensive hardware and generates images at a lower sensitivity. Recently, another solution has been proposed by [8], which uses a continuously-moving ultrasound probe. The probe is moved back and forth with a sinusoidal trajectory throughout the experiment, resulting in a 3D volume after every half-cycle of the probe's movement (called as a *passover*). As such, computing the voxel-power from consecutive compound images (as in the 2D case) would require integrating over different slices, and ignoring the spatial changes within the batch. Furthermore, due to the sinusoidal motion of the probe, compound images are recorded ~ 10 times slower at the extremities of the trajectory. Thus, using a similar batch size as in the 2D case to obtain PDIs would mean integrating over a much larger period in time. All in all, following the same settings as used for 2D fUS could neglect important changes along both space and time in swept-3D fUS imaging.

In fMRI literature, slice offset problem is commonly addressed under the term *slice-timing correction*. However, for fMRI, as the name suggests, the only problem is the temporal offset between slices. On the other hand, for swept-3D fUS, PDI computation demands averaging over a number of transmissions; which also vary in space due to the probe's motion. Therefore, even if temporal alignment of slices is achieved (such as using interpolation techniques, [9]), spatial changes would still be ignored within a batch. Nevertheless, we can consider a limit under which such spatiotemporal variation can be regarded as insignificant, in other words, a number of frames for which PDI-computation would be "safe". We discuss this limit further in Section 5.

Our goal is to recover functional response while preserving the spatiotemporal differences amongst PDIs, which are created using fewer compound frames. However, the fewer compound frames used for computing PDIs, the more PDIs suffer from poor signal-to-noise-ratio (SNR). Hence, we ex-

ploit prior information introduced via a general linear model (GLM)-based regularization to unravel the task-related content from low-SNR PDIs. To that end, we apply low-rank decomposition on the fUS data matrix -which we formulate as incomplete to model probe motion- using alternating minimization (AM) [10] with sparse GLM-regularization [11].

The rest of this paper is organized as follows. We first explain our problem formulation and the proposed solution. We then present our results in simulations and in-vivo swept-3D fUS data, which we compare with standard analysis.

2. PROBLEM FORMULATION

The acquired swept-3D fUS data is naturally a 4D space-time array of size $N_z \times N_x \times N_y \times T$, where N_z, N_x and N_y represent the number of voxels in depth, width and height respectively, whereas T is the total number of time samples. Due to the motion of the probe, a 2D image of size $N_z \times N_x$ is acquired at each time sample, corresponding to a slice at $y-$axis. Thus, by vectorizing the space dimension, we can obtain a 2D matrix $\mathbf{Y}$ of size $N_z N_x N_y \times T$ representing the acquired fUS data, as shown in Fig. 1. The blank parts of Fig. 1 simply refer to points of no acquisition. We will denote the observed entries by the set $\Omega = \{(i,j) : \mathbf{Y}_{ij} \text{ is observed}\}$.

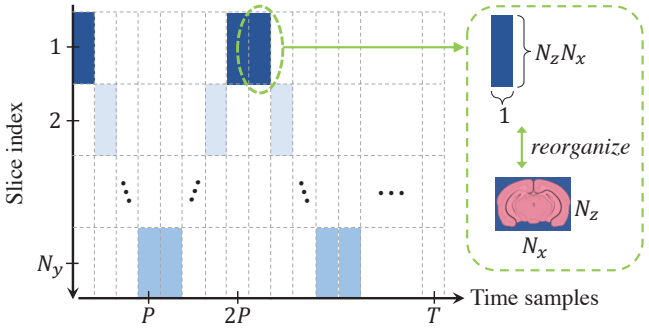

Fig. 1: Matrix representation of swept-3D fUS data. Each colored block stands for an imaged brain slice in vectorized format. P denotes the time for one passover.

We hypothesize that $\mathbf{Y}$ can be successfully decomposed to reveal task-relevant information from fUS data only based on its observed elements using a low-rank approximation [12]. More specifically, we factorize the fUS data matrix into its space and time components, each represented as a rank-2 matrix. We purposefully opt for a rank-2 representation to model all the task-related content together in one component ([13]), while the second component accounts for the remaining activity. We ensure this separation by applying a GLM regularization to a single column of the factor matrix in time, which will capture the HRF-mediated content of interest from fUS data. To employ the GLM regularization, we construct several response variables by convolving different HRF shapes with the known stimulus time course (i.e., the binary input signal which shows the on- and off- times of the stimulus). While all the results in this study are obtained with $R = 2$, we will present the proposed method using a rank-R decomposition for the sake of generalizability.

The problem that we aim to solve can be expressed as:

$$(\hat{\mathbf{U}}, \hat{\mathbf{V}}, \hat{\boldsymbol{\beta}}) = \underset{(\mathbf{U},\mathbf{V},\boldsymbol{\beta})}{\operatorname{argmin}} \|\mathbf{Y}_{(i,j)\in\Omega} - [\mathbf{U}\mathbf{V}^{\mathrm{T}}]_{(i,j)\in\Omega}\|_{\mathrm{F}}^2 + \lambda_1 \|\mathbf{V}_{:,1} - \mathbf{X}\boldsymbol{\beta}\|_{\mathrm{F}}^2 + \lambda_2 \|\boldsymbol{\beta}\|_1, \quad (1)$$

where $\hat{\mathbf{U}} \in \mathbb{R}^{N_z N_x N_y \times R}$ and $\hat{\mathbf{V}} \in \mathbb{R}^{T \times R}$ are rank-R factor matrices containing the spatial and temporal signatures of $\mathbf{Y}$ respectively, and $\mathbf{V}_{:,1}$ refers to the first column of $\mathbf{V}$. Note that, applying GLM-regularization to a single column of $\mathbf{V}$ allows for task-related content to be solely captured in that component, whereas the second component models the rest, i.e. background activity. For more complex experimental designs, such as when multiple tasks are incorporated, higher-rank models can be used where every column of V would refer to the onsets of a specific stimulus. $\mathbf{X} \in \mathbb{R}^{T \times B}$ is the design matrix, whose columns correspond to the regressors obtained by convolving different HRF shapes with the stimulus vector. B, the number of columns of $\mathbf{X}$, is the number of basis functions (or the HRF shapes) to be incorporated. HRFs used in this work (generated using the gamma model, [2]) are shown in Fig. 2. $\boldsymbol{\beta} \in \mathbb{R}^{B \times 1}$ stores the regression coefficients, i.e. the contribution of each design matrix column. We assume that $\boldsymbol{\beta}$ is sparse to reveal physiologically-meaningful HRF shapes. $\|.\|_{\mathrm{F}}$ is the Frobenius norm and $\|.\|_1$ is the l_1-norm. The regularization coefficients λ_1 and λ_2, adjust the influence of GLM and sparsity of the regression coefficients respectively. Eq. 1 gives an estimate of the factor matrices in time and space, as well as the HRF.

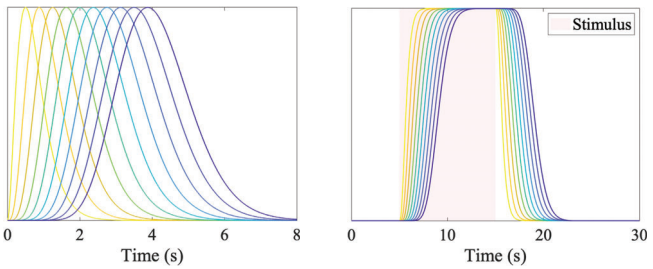

(a) (b)

Fig. 2: The HRFs used in this work (a) and columns of an example design matrix obtained by convolving a simulated 10-second stimulus with the HRFs (b).

3. PROPOSED METHOD

Although the problem stated in Eq. 1 is not jointly convex in $\mathbf{U}$, $\mathbf{V}$ and $\boldsymbol{\beta}$, it can be reformulated as such by alternating the optimization between them [14]. Steps of the proposed three-way AM approach are elaborated in Algorithm 1, where ϵ is the error threshold for determining the point of convergence. We solve the presented AM scheme using the CVX package [15] in MATLAB. All codes are made publicly available[1].

[1] https://github.com/ayerol/GLMR_Swept_3DfUS

Algorithm 1 Steps of the proposed AM algorithm.

Inputs: $\mathbf{Y}, \mathbf{X}$

Initialize: $\boldsymbol{\beta}^{(0)} \leftarrow \mathbf{e}_1, \mathbf{V}_{:,1}^{(0)} \leftarrow \mathbf{X}\boldsymbol{\beta}^{(0)}, \mathbf{V}_{:,2}^{(0)} \leftarrow \mathcal{U}(0,1)$, $k = 0, \lambda_1, \lambda_2, \epsilon$

while $\|\mathbf{U}^{(k+1)} - \mathbf{U}^{(k)}\|_{\mathrm{F}}^2 + \|\mathbf{V}^{(k+1)} - \mathbf{V}^{(k)}\|_{\mathrm{F}}^2 > \epsilon$ **do**

$$\mathbf{U}^{(k+1)} \leftarrow \underset{\mathbf{U}}{\operatorname{argmin}} \|\mathbf{Y}_{(i,j)\in\Omega} - [\mathbf{U}\mathbf{V}^{(k)^{\mathrm{T}}}]_{(i,j)\in\Omega}\|_{\mathrm{F}}^2 \quad (2)$$

$$\mathbf{V}^{(k+1)} \leftarrow \underset{\mathbf{V}}{\operatorname{argmin}} \|\mathbf{Y}_{(i,j)\in\Omega} - [\mathbf{U}^{(k)}\mathbf{V}^{\mathrm{T}}]_{(i,j)\in\Omega}\|_{\mathrm{F}}^2 + \lambda_1^{(k)}\|\mathbf{V}_{:,1} - \mathbf{X}\boldsymbol{\beta}^{(k)}\|_{\mathrm{F}}^2 \quad (3)$$

$$\boldsymbol{\beta}^{(k+1)} \leftarrow \underset{\boldsymbol{\beta}}{\operatorname{argmin}} \lambda_1^{(k)}\|\mathbf{V}_{:,1}^{(k)} - \mathbf{X}\boldsymbol{\beta}\|_{\mathrm{F}}^2 + \lambda_2^{(k)}\|\boldsymbol{\beta}\|_1 \quad (4)$$

$k \leftarrow k + 1$

end while

Outputs: $\mathbf{U}, \mathbf{V}, \boldsymbol{\beta}$

4. SIMULATIONS

We simulated a 3D brain of size (20,20,20) with two regions-of-interest (ROIs). We assumed that there is one common task that evokes activity in the ROIs, and we modelled this task using the same stimulus times as in the real fUS experiment (Section 5), representing it as a binary signal (1 when the stimulus is on). To construct the task-induced time-course, we convolved the stimulus signal with an HRF. We assumed that the strength of this task-induced time-course varies smoothly within the ROIs, such that it is highest at their center, as controlled by the HRF peak amplitude (Fig. 3(a)). Next, we simulated another time-course to represent background activity, which we generated as a normally distributed sequence. We also introduced a sudden rise in the baseline of this activity to mimic head motion artifacts [16]. Unlike the task-induced response (which is present only in ROIs), we assumed that the background activity is observed in the whole brain, yet with a different strength at each voxel. Specifically, we set the voxel-scaling of the background activity randomly from a uniform distribution $\mathcal{U}(0.5, 1)$. Lastly, we assumed that only one slice is measured at a time to model probe motion.

Results are shown in Fig. 4. As expected, we see that the GLM-regularized component reflects the task-related content both in space and time. On the other hand, the second component models the remainder of the data, corresponding to the noisy background activity with motion artifacts. We can appreciate that while the first spatial signature is mostly zero outside the ROIs, the second signature is distributed homogeneously throughout the brain, indicating commonality.

5. fUS RESULTS

We acquired the fUS data from a head-fixed C57BL/6 mouse through a craniotomy [8]. The mouse was presented with a series of LED stimuli, flickering at 3 Hz during the on-periods. Each repetition of the stimulus was kept on for a random duration between [5,12] s, followed by a random rest period of

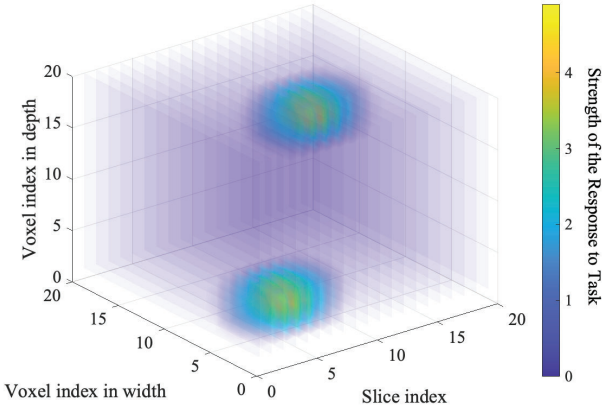

(a) Simulated brain with two ROIs. The colormap indicates the per-voxel response strength given to the stimulus.

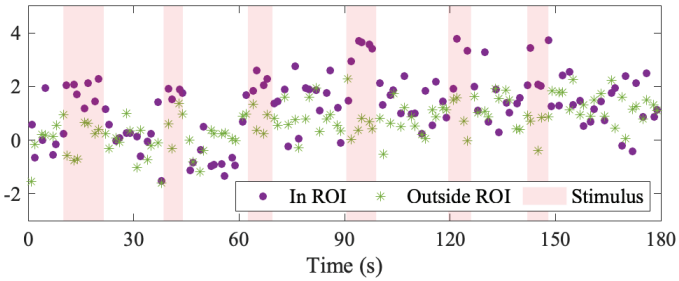

(b) Two example responses generated within and outside a ROI. Motion takes place around the 60th second.

Fig. 3: Simulated data.

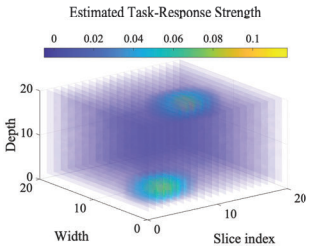

(a) First spatial signature.

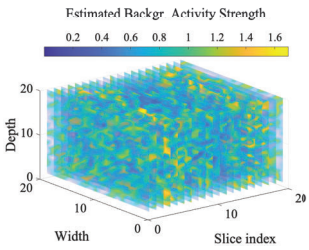

(b) Second spatial signature.

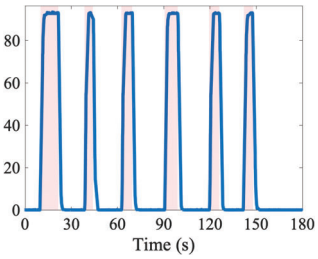

(c) First temporal signature.

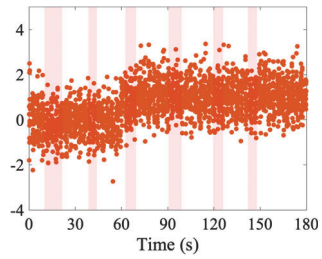

(d) Second temporal signature.

Fig. 4: Simulation results. The first component ((a) and (c)) is GLM-regularized, thus, models the task-relevant content, while the second component ((b) and (d)) depicts background activity. Note that, the temporal resolution in (c)-(d) is higher than the number of samples per-voxel (Fig. 3(b)), which is a result of missing entries being filled after decomposition.

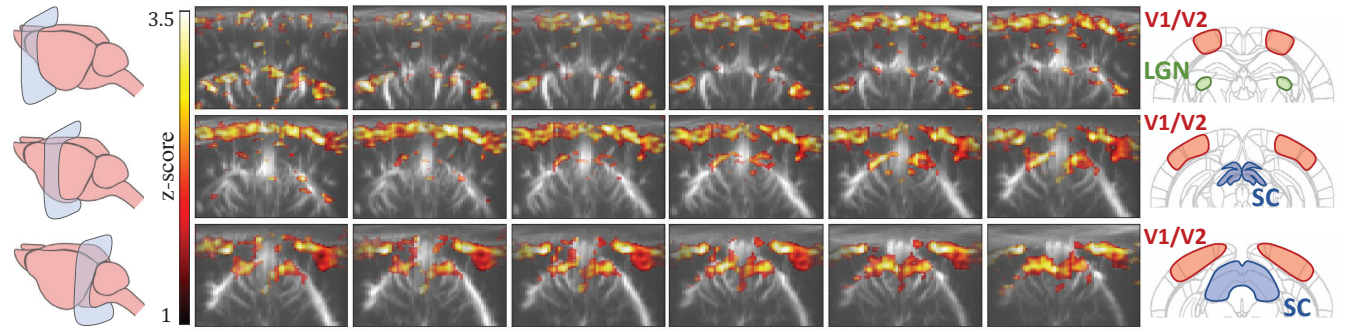

Fig. 5: Estimated activation maps. All the images span a depth of [0.5,4] mm and a width of [-3,3] mm. Slices are equally spaced and range from Bregma -1 to -4 mm. We only put schematic views for 3 slices (left and right columns), each corresponding to the mean slice of a row. Highlighted regions at the right column show the key visual information processing regions of the mouse brain: the superior colliculus (SC), lateral geniculate nucleus (LGN) and visual cortex (V1/V2).

[15,25] s. A high-frequency linear array transducer (L22-14v) was attached to a motorized stage (Zaber X-LDA025A), moving in a sinusodial trajectory with a period of ~ 3 s, and coupled to a Verasonics acquisition system. Plane waves were transmitted at 8 angles ($\pm 9°$) and beamformed in Fourier-domain. We applied SVD-filtering to the beamformed frames of a full passover to reject tissue motion artifacts. To construct PDIs, we selected our batch size according to a spatiotemporal limit, for which stationarity can be assumed in both domains. In space, we used the Allen Mouse Brain Atlas [17] resolution as our reference, where each coronal slice is distanced 0.1 mm apart. For time, we referred to the original batch duration used in 2D fUS, that is 0.2 s [5]. In the end, we obtained PDIs using only 30 compound frames (non-overlapping), corresponding to a time window of ~ 0.15 s towards the ends of the brain, and ~ 0.03 s in the middle parts; and a scanning distance of 0.13 mm. We would like to emphasize that our final fUS data matrix $\mathbf{Y}$ is in the form shown in Fig 1, where each block-entry is a PDI. Lastly, we standardized all voxel time-series (to zero-mean and unit variance) and applied spatial smoothing with a 3D Gaussian kernel with standard deviation corresponding to one voxel.

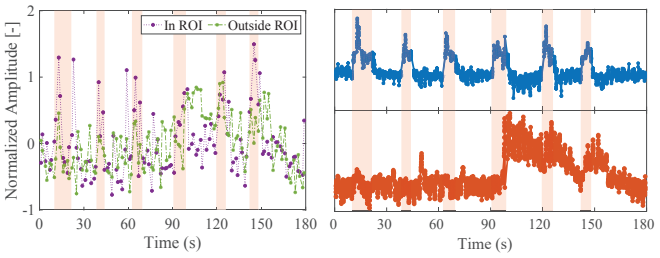

(a) Two example voxel time-series (ROI here refers to SC).

(b) First (top) and second (bottom) estimated temporal signatures.

Fig. 6: 3D-fUS results in time.

The results shown in Fig. 6 reveal that the second temporal signature captures the noisy content (including motion artifacts) of fUS data, while the GLM-regularized signature models the stimulus-led activity. To compare the performance of our method with standard approaches, we calculated the highest z-score at each ROI as an indication of how well the ROI response is differentiated from the background. We applied the same process for activation maps obtained via voxel-wise correlations and standard GLM. For the latter, we interpolated each voxel time-series according to a common time axis, and used two regressors following [18] for the design matrix: one is obtained with convolving the stimulus signal with an HRF (for which we used the optimal HRF found by our method); whereas the other is a constant. The results are provided in Table 1, confirming that our method achieves the highest contrast between active and non-active brain areas.

ROI	Correlation	Standard GLM [18]	Our Method
SC	2.9	3.5	**3.7**
LGN	**2.9**	2.8	**2.9**
V1/V2	2.8	2.9	**3.2**

Table 1: Highest z-scores achieved at each ROI.

6. CONCLUSION

In this work, we aimed at unravelling the task-related components of the brain from swept-3D fUS data obtained via a continuously moving ultrasound probe, resulting in an incomplete data matrix. The proposed method aims at recovering the spatiotemporal content of interest from fUS data by defining explanatory variables via a GLM. We propose an alternating convex optimization scheme with GLM-regularization to decompose the data into its low-rank components. We first validate our approach on synthetic data, and later compare our results on in-vivo fUS data with conventional analyses. Our results reveal that we are able to uncover more significant activations in functional brain regions compared to conventional methods. In the future, we plan to investigate higher-rank models to incorporate multiple experimental paradigms.

7. REFERENCES

[1] T. Deffieux, C. Demené, and M. Tanter, "Functional ultrasound imaging: A new imaging modality for neuroscience," *Neuroscience*, vol. 474, pp. 110–121, 2021.

[2] A. Erol, C. Soloukey, B. Generowicz, N. Van Dorp, S. Koekkoek, P. Kruizinga, and B. Hunyadi, "Deconvolution of the functional ultrasound response in the mouse visual pathway using block-term decomposition," *Neuroinformatics*, 2022.

[3] A.O. Nunez-Elizalde, M. Krumin, C B. Reddy, G. Montaldo, A. Urban, K.D. Harris, and M. Carandini, "Neural correlates of blood flow measured by ultrasound," *Neuron*, vol. 110, no. 10, pp. 1631–1640.e4, 2022.

[4] C. Demené, T. Deffieux, M. Pernot, B.F. Osmanski, V. Biran, J.L. Gennisson, L.A. Sieu, A. Bergel, S. Franqui, J.M. Correas, et al., "Spatiotemporal clutter filtering of ultrafast ultrasound data highly increases Doppler and fUltrasound sensitivity," *IEEE Transactions on Medical Imaging*, vol. 34, no. 11, pp. 2271–2285, 2015.

[5] E. Macé, G. Montaldo, I. Cohen, M. Baulac, M. Fink, and M. Tanter, "Functional ultrasound imaging of the brain," *Nature Methods*, vol. 8, no. 8, pp. 662–664, 2011.

[6] R. Rau, P. Kruizinga, F. Mastik, M. Belau, N. de Jong, J.G. Bosch, W. Scheffer, and G. Maret, "3D functional ultrasound imaging of pigeons," *Neuroimage*, vol. 183, pp. 469–477, 2018.

[7] J. Sauvage, J. Porée, C. Rabut, G. Férin, M. Flesch, B. Rosinski, A. Nguyen-Dinh, M. Tanter, M. Pernot, and T. Deffieux, "4D functional imaging of the rat brain using a large aperture row-column array," *IEEE Transactions on Medical Imaging*, vol. 39, no. 6, pp. 1884–1893, 2019.

[8] B. Generowicz, S. Dijkhuizen, C. De Zeeuw, S. Koekkoek, and P. Kruizinga, "3D functional ultrasound using a continuously moving linear stage," in *2022 IEEE International Ultrasonics Symposium (IUS)*, 2022, pp. 1–3.

[9] D. Parker, X. Liu, and Q.R. Razlighi, "Optimal slice timing correction and its interaction with fMRI parameters and artifacts," *Medical Image Analysis*, vol. 35, pp. 434–445, 2017.

[10] H. Cherkaoui, T. Moreau, A. Halimi, and P. Ciuciu, "Sparsity-based blind deconvolution of neural activation signal in fMRI," in *IEEE International Conference on Acoustics, Speech and Signal Processing (ICASSP)*. IEEE, 2019, pp. 1323–1327.

[11] Y. Li, P. Namburi, Z. Yu, C. Guan, J. Feng, and Z. Gu, "Voxel selection in fMRI data analysis based on sparse representation," *IEEE Transactions on Biomedical Engineering*, vol. 56, no. 10, pp. 2439–2451, 2009.

[12] T. Hastie, R. Mazumder, J. D. Lee, and R. Zadeh, "Matrix completion and low-rank SVD via fast alternating least squares," *The Journal of Machine Learning Research*, vol. 16, no. 1, pp. 3367–3402, 2015.

[13] P.A. Karakasis, A.P. Liavas, N.D. Sidiropoulos, P.G. Simos, and E. Papadaki, "Multisubject task-related fMRI data processing via a two-stage generalized canonical correlation analysis," *IEEE Transactions on Image Processing*, vol. 31, pp. 4011–4022, 2022.

[14] P. Jain, P. Netrapalli, and S. Sanghavi, "Low-rank matrix completion using alternating minimization," *Proceedings of the Annual ACM Symposium on Theory of Computing*, pp. 665–674, 2012.

[15] M. Grant and S. Boyd, "CVX: Matlab software for disciplined convex programming, version 2.1," `http://cvxr.com/cvx`, Mar. 2014.

[16] N. Correa, T. Adali, Yi-Ou Li, and V.D. Calhoun, "Comparison of blind source separation algorithms for FMRI using a new Matlab toolbox: GIFT," in *Proceedings. (ICASSP '05). IEEE International Conference on Acoustics, Speech, and Signal Processing, 2005.*, 2005, vol. 5, pp. v/401–v/404 Vol. 5.

[17] Allen Institute for Brain Science, "Allen Brain Atlas API," 2015, Available from: `brain-map.org/api/index.html`.

[18] C. Brunner, M. Grillet, A. Urban, B. Roska, G. Montaldo, and E. Macé, "Whole-brain functional ultrasound imaging in awake head-fixed mice," *Nature Protocols*, vol. 16, no. 7, pp. 3547–3571, 2021.